Supplementary information for "Parallel electron-hole bilayer conductivity from electronic interface reconstruction"

R. Pentcheva,[1] M. Huijben,[2] K. Otte,[1] W.E. Pickett,[3] J.E. Kleibeuker,[2] J. Huijben,[2] H. Boschker,[2] D. Kockmann,[2] W. Siemons,[4] G. Koster,[2] H.J.W. Zandvliet,[2] G. Rijnders,[2] D.H.A. Blank,[2] H. Hilgenkamp,[2] and A. Brinkman[2]

[1]*Department of Earth and Environmental Sciences, University of Munich, Germany*
[2]*Faculty of Science and Technology and MESA+ Institute for Nanotechnology, University of Twente, The Netherlands*
[3]*Department of Physics, University of California, Davis, USA*
[4]*Department of Physics, University of California, Berkeley, USA*

EVOLUTION OF DENSITY OF STATES

Figure 1 shows the evolution of the total density of states (DOS) as a function of the number, m, of STO capping layers in STO(001)/2LAO/mSTO samples. While the first layer has the dominating effect of reducing the band gap by 1.2 eV, a second STO layer leads to a clear band overlap and an enhancement of the DOS at the Fermi level.

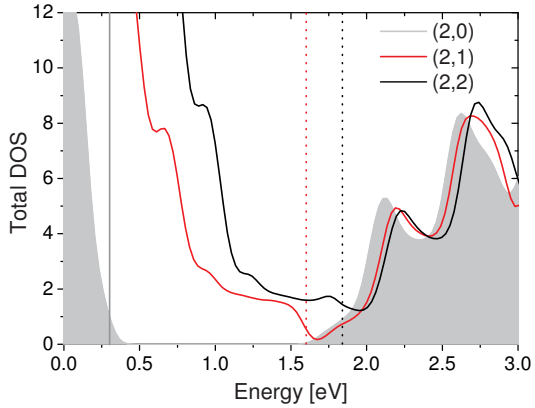

FIG. 1: Total density of states (DOS) of STO(001)/2LAO/mSTO, aligned at the bottom of the Ti $3d$ band at the interface. Vertical lines mark the positions of the Fermi level for each system. By adding a STO capping layer, the band gap of STO(001)/2LAO is reduced by 1.2 eV. Further capping layers lead to an increase of DOS at the Fermi level.

IONIC RELAXATIONS

Figure 2 shows the calculated layer resolved ionic displacements [1] in STO(001)/2LAO/mSTO. Additionally, the relaxations of a STO(001)-surface are plotted. For the uncapped systems Al and O both relax inwards by similar amounts without a ferroelectric distortion. In contrast, there is a strong buckling in the surface TiO_2 layer in the case of STO capping. The relaxation pattern in the capping layers bears a striking resemblance to the structure of the STO(001) surface, where the total dipole is relatively small $D_{ionic}^{\mathrm{STO(001)}} = -0.19$ eÅ [2]. As mentioned previously, also the electronic structure of the

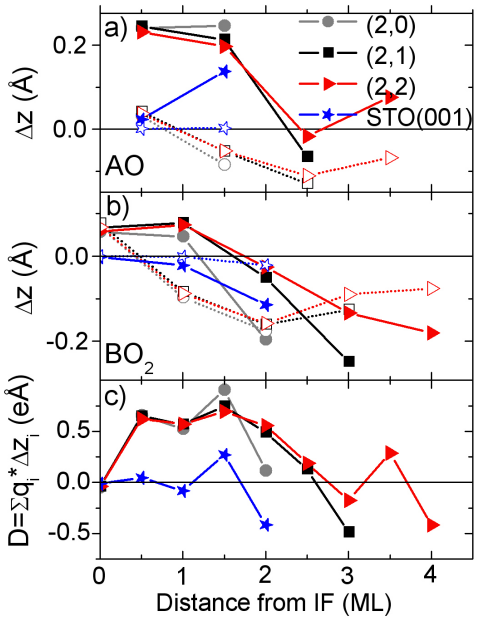

FIG. 2: Ionic relaxations in STO(001)/2LAO/mSTO and the bare STO(001)-surface. Vertical displacements Δz are shown with respect to the bulk position in the (a) AO and (b) BO_2 layers, (c) layer-resolved dipole moments as a function of the distance from the interface (IF) TiO_2-layer. The filled (open) symbols mark cation (anion) relaxations. (n, m) denotes the number n of LAO and m of STO layers in the respective system.

STO(001) surface [3, 4] and the capping layer are similar, in particular a dispersive O $2p$ surface state with maximum at the M-point appears. Due to the small ionic contribution of the capping layer the total dipole moment is not affected appreciably by the capping layer: $D_{ionic}^{(2,0)} = 2.15$ eÅ, $D_{ionic}^{(2,1)} = 2.05$ eÅ, and $D_{ionic}^{(2,2)} = 2.28$ eÅ. The latter turns out to be determined by the total number of LAO layers, *e.g.* $D_{ionic}^{(1,1)} = 1.02$ eÅ, $D_{ionic}^{(2,1)} = 2.05$ eÅ, and $D_{ionic}^{(3,1)} = 3.30$ eÅ.

SPECTROSCOPIC DETAILS

Figure 3 shows the current-voltage tunneling characteristics of a STO(001)/2LAO/1STO sample and the derived normal-

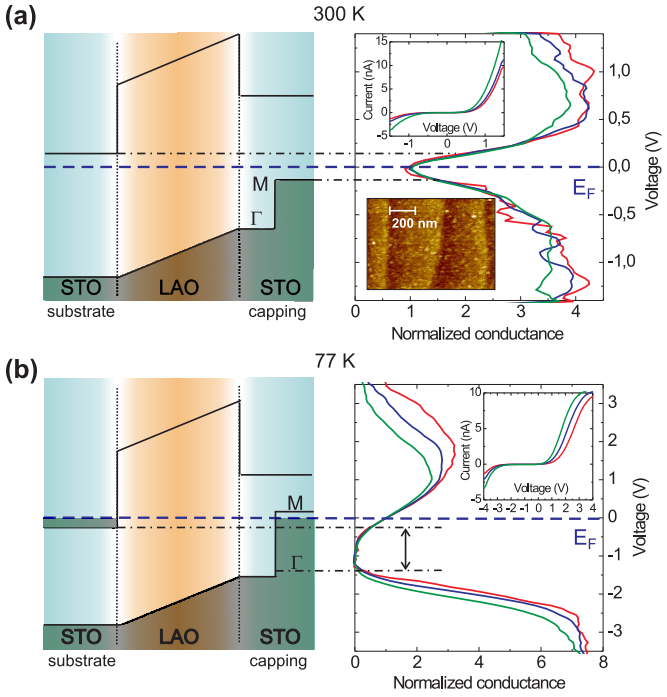

FIG. 3: (a) Scanning tunneling normalized conductance $(dI/dV)/(I/V)$ measurements of a STO(001)/2LAO/1STO sample at 300 K for different tip-sample distances (current set-point respectively 1.5 nA, 2.0 nA, and 4.0 nA at a bias voltage of -1.5 V). The schematic drawing explains the small gap between the valence band at the M-point of the STO capping surface and the conduction band at the substrate-LAO interface. The Fermi energy, E_F, at $V = 0$ V (blue dashed line) lies in the gap. The upper inset shows the current-voltage characteristics from which the conductance was derived and the lower inset shows an STM topography image taken at 300 K with a bias voltage of -1.0 V. (b) Normalized conductance at 77 K (current set-point respectively 1.5 nA, 2.5 nA, and 4.0 nA at a bias voltage of -4.0 V). The schematic drawing explains the larger gap between the valence band Γ point at the STO capping surface and the substrate-LAO interface conduction band. The Fermi energy (blue dashed line) lies now in the conduction band. Band bending is not depicted on this scale. The inset shows the current-voltage characteristics.

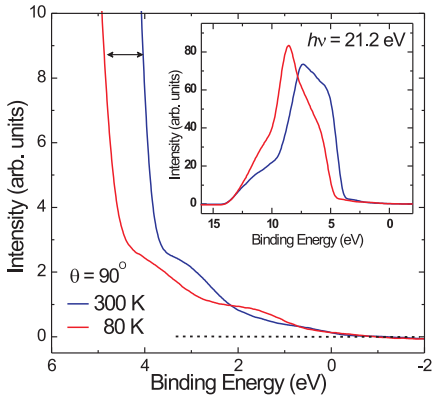

FIG. 4: UPS spectra of a STO(001)/2LAO/1STO sample taken *in situ* after growth, at 300 K and 80 K with the detector at 90°. The inset shows the zoomed-out full spectra. The data has been normalized to the integrated peak height. The arrows indicate a significant shift that was observed between the spectra.

ized conductivity $(dI/dV)/(I/V)$, which can be interpreted as the sample local density of states (LDOS). Assuming that tunneling occurs both to the surface and to the substrate-LAO interface, these spectroscopic features can be understood on the basis of the band structure calculations. At 300 K, the Fermi energy lies between the valence band at the M-point in the surface and the conduction band at the Γ-point in the substrate-LAO interface. At 77 K, see Fig. 3b, the valence band seems to have shifted to lower energy. We will elaborate below that this is due to the momentum-resolving capabilities of STS.

The apparent increase of the STS band gap when cooling down from room temperature to 77 K can be understood from an analysis of measurements of the tunnel current, I, versus the tip-sample separation, z, at fixed (negative) sample bias. The tunnel current $I \propto e^{-2\kappa z}$ is measured at negative sample biases in the range from -1 V to -3 V. The inverse decay length, κ, is substantially larger at room temperature ($\sim$ 80 %) than at 77 K. The inverse decay length is given by $\kappa = \sqrt{C + k_{\parallel}^2}$, where C only depends on the temperature independent tunnel barrier height and $k_{\parallel}$ is the parallel momentum of the surface electronic structure [5]. The relatively large κ at room temperature strongly supports the idea that at room temperature tunneling occurs from filled surface electronic states with a nonzero parallel momentum (*i.e.* regions near the M point of the surface Brillouin zone) to empty states of the tip. Accordingly, at 77 K tunneling mainly occurs from filled electronic states near the Γ point of the surface Brillouin zone to empty states of the tip, leading to substantial increase of the measured band gap. The latter analysis emphasizes that the electrons that are transferred across the STO/LAO/STO structure upon reconstruction indeed originate from the M point of the surface STO Brillouin zone.

The STS measurements also reveal that, upon lowering the temperature, the Fermi energy is slightly shifted to higher energies. At 77 K, E_F is found to ly in the conduction band. This finding was confirmed by the temperature dependence of the UPS spectra. While the overall spectra (see inset of Fig. 4) resemble those for bulk STO [6], a clear 1 eV peak shift to higher binding energy is observed for 80 K when compared to 300 K. This can be interpreted as an upward shift of the Fermi energy relative to the valence band maximum in the bulk of STO when lowering the temperature, analogous to the observation by STS.

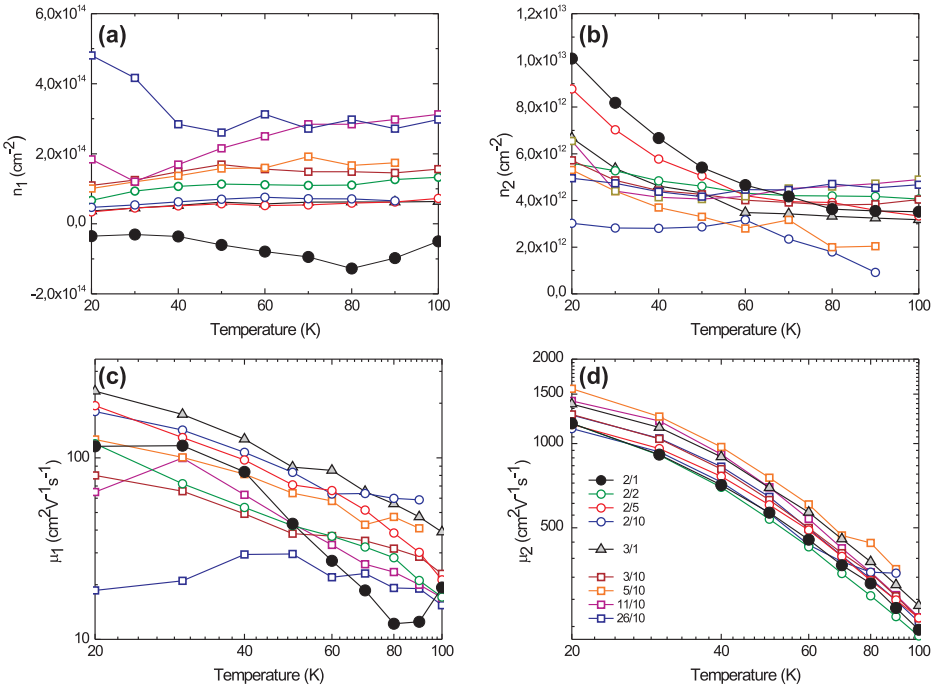

FIG. 5: Two-band fitting results for different STO(001)/nLAO/mSTO samples. The magnetoresistance and Hall effect field dependence were fitted with a two-band model. The fitting provides two carrier densities (a-b) and two mobilities (c-d) for each n/m sample.

TWO-BAND FITTING RESULTS

For every electronic band n, that contributes to conductivity, the induced current $\boldsymbol{j_n}$ is given by the electric field $\boldsymbol{E_n}$ times the band conductivity $\boldsymbol{\sigma_n}$, $\boldsymbol{j_n} = \boldsymbol{\sigma_n E_n}$. The band resistivity $\boldsymbol{\rho_n} = \boldsymbol{\sigma_n^{-1}}$ is defined as

$$\boldsymbol{\rho_n} = \begin{pmatrix} \rho_n & -R_n H \\ R_n H & \rho_n \end{pmatrix}, \tag{1}$$

where ρ_n is the longitudinal resistance, R_n the transverse Hall coefficient and H the magnetic field. The *total* resistivity tensor $\boldsymbol{\rho}$, defined as

$$\boldsymbol{\rho_n} = \begin{pmatrix} \rho & -RH \\ RH & \rho \end{pmatrix}, \tag{2}$$

is given by $\boldsymbol{\rho} = \boldsymbol{\sigma}^{-1} = \left(\sum_n \boldsymbol{\sigma_n}\right)^{-1} = \left(\sum_n \boldsymbol{\rho_n^{-1}}\right)^{-1}$. When only two bands contribute to conductivity, it follows that the total longitudinal and Hall resistances can be expressed as

$$\rho = \frac{\rho_0 + \rho_\infty \mu^2 H^2}{1 + \mu^2 H^2}, \tag{3}$$

$$R_H = \frac{R_0 + R_\infty \mu^2 H^2}{1 + \mu^2 H^2}, \tag{4}$$

where $R_0 = \left(R_1\sigma_1^2 + R_2\sigma_2^2\right)(\sigma_1+\sigma_2)^{-2}$, $R_\infty = R_1 R_2 (R_1+R_2)^{-1}$, $\mu = (R_1+R_2)\,\sigma_1\sigma_2\,(\sigma_1+\sigma_2)^{-1}$, $\rho_0 = (\sigma_1+\sigma_2)^{-1}$, and $\rho_\infty = \left(R_1^2\sigma_2^{-1} + R_2^2\sigma_1^{-1}\right)(R_1+R_2)^{-2}$.

The band conductivities are given by $\sigma_{1,2} = |n_{1,2}|\,\mu_{1,2}$ and the band Hall resistivities by $R_{1,2} = (n_{1,2})^{-1}$, where n is negative for electrons (negative curvature in the band dispersion relation) and positive for holes (positive band curvature).

Equations (3) and (4) were fitted simultaneously to the measured sheet resistance and Hall resistance by means of a least square fitting routine. The resistivity data was symmetrized (average over values at positive and negative fields) in order to exclude a transverse resistance contribution to the longitudinal resistance. The Hall resistivity was anti-symmetrized (difference between values at positive and negative fields) in order to exclude longitudinal components. All the different samples could be fitted within the experimental error bars. The results for all measured STO(001)/nLAO/mSTO samples are shown in Fig. 5.

[1] The DFT calculations are performed in a tetragonal unit cell with a full relaxation of the vertical positions of the atoms. Further distortions such as tilting and rotations of the octahedra have not been included and are assumed not to be relevant to our main conclusions. Due to the small occupation of the Ti $3d$ band no further symmetry lowering is observed by using a larger lateral periodicity in a $c(2\times 2)$ unit cell.

[2] The dipole moment is determined from the ionic displacements using the formal ionic charges. Although Born effective charges may be more appropriate, we use this approach as a rough estimate of the ionic contribution to the total dipole.

[3] S. Kimura, J. Yamauchi, M. Tsukada, S. Watanabe, Phys. Rev. B

51, 11049 (1995).
[4] J. Padilla, D. Vanderbilt, Surf. Sci. **418**, 64 (1998).
[5] H.J.W. Zandvliet, A. van Houselt, Ann. Rev. Anal. Chem. **2**, 37 (2009).
[6] W. Siemons *et al.*, Phys. Rev. B **76**, 155111 (2007).